

We are IntechOpen, the world's leading publisher of Open Access books Built by scientists, for scientists

6,900

Open access books available

185,000

International authors and editors

200M

Downloads

Our authors are among the

154

Countries delivered to

TOP 1%

most cited scientists

12.2%

Contributors from top 500 universities



WEB OF SCIENCE™

Selection of our books indexed in the Book Citation Index
in Web of Science™ Core Collection (BKCI)

Interested in publishing with us?
Contact book.department@intechopen.com

Numbers displayed above are based on latest data collected.
For more information visit www.intechopen.com



Recent Advances in Coastal Survey Techniques: From GNSS to LiDAR and Digital Photogrammetry - Examples on the Northern Coast of France

Olivier Cohen and Arnaud Héquette

Abstract

The aim of this chapter is to document the evolution of surveying techniques used for monitoring changes in morphology of beaches and coastal dunes in northern France, beginning with GNSS surveys in the 1990s, followed by airborne topographic LiDAR surveys since 2008, and high-resolution digital photogrammetry data collected by an UAV during recent years. Digital Terrain Models (DTMs) derived from the data obtained from the different techniques were used for monitoring coastal changes, including shoreline evolution, and for computing sediment volume changes across the foreshore and the coastal dunes at different time and spatial scales. A comparison of the results obtained using these different techniques and of their accuracy will be carried out to assess the pro and cons of each surveying technique.

Keywords: GNSS, LiDAR, UAV, topographic survey, digital elevation models, coastal geomorphology, northern coast of France, shoreline evolution, sediment budget

1. Introduction: from a classical naturalistic approach to a contemporary quantitative approach

Research in coastal geomorphology aims at describing the shapes of coastal landforms (dunes, beaches, cliffs, estuaries, deltas, shorefaces, etc.) at different temporal scales (long to short term, several thousand years to a few hours) and spatial scales (over large to small areas) and understanding the processes of their evolution [1, 2]. This research is frequently applied to the study of risks, for example, in case of shoreline erosion, the evolution of the coastline is mapped, and sediment budgets are calculated to define the hazards threatening human infrastructures.

Many methods are used to detect shoreline changes. They can be classified into three categories depending on the date and duration of the study period and the type of tools used [3].

To map the medium-term coastline evolution from secular to multi-decadal scale and in two dimensions (in plan), diachronic analysis of historic maps, aerial

photographs since the mid-twentieth century, and more recent high spatial resolution satellite images are often used. On historic maps that are often imprecise in their drawing, it usually results in approximate measurements. However, they represent valuable documents for a qualitative or naturalistic geo-historic analysis of landscape [3, 4]. On these maps published since the end of the nineteenth century and on vertical aerial photographs available since the 1930s, the successive positions of the coastline can be identified, digitized, and then compared in a Geographical Information Systems (e.g., [5–7]) in order to determine erosion or accretion zones.

Within the second category of methods, in the shorter term, over the last 30 years or so, measurements have been carried out in two ways with high-tech instruments. First, geodetic instruments (e.g., total electronic stations and GNSS) are used to carry out data collection in the field. These measurements are time-consuming and difficult to carry out over large areas; only a fairly limited number of points can be acquired (a few hundred to a few thousand); therefore, only beach profiles (cross section of the range from a few tens to hundreds of meters long) or Digital Terrain Models (DTM) of limited size (a few thousand square meters) and low spatial resolution can be surveyed. Second, also in the short term, telemetry instruments (e.g., ground or airborne LiDAR) that enable the rapid collection of a large amount of elevation data that are transformed into DTM are used.

The third category encompasses the methods of photogrammetric processing that allow to extract elevation data from aerial photographs; this technique also allows to collect a very large amount of data that are transformed into Digital Surface Model (DSM).

The evolution of these techniques can also be conceptualized in a “measurement method paradigm” (**Figure 1**): with the methods of the first category, we start from the images to make measurements. Paper images (maps or aerial photographs) available in paper format are scanned or acquired directly in digital format; geometric deformations are corrected, and they are georeferenced; measurements are then carried out and statistically processed. It should be noted here that the analysis is in two dimensions (in plan). With the methods of the second category, measurements are performed and transformed into images (DTM and DSM), which are the result of calculations and not a direct capture of the reality of the terrain. One of the major interests of these methods is to be able to work in three dimensions: the measurements made are in plan and in altitude. The third category closes the paradigm: the work process starts with images (aerial photographs), continues with measurements, and returns to images (DSM). Here, the analysis is also in three dimensions.

This paradigm has undergone a twofold evolution over the last 25 years or so. First, the transition from 2D to 3D measurements has been a determining factor in coastal geomorphology. This has made it possible to objectify the position of the coastline, which is not always easy to detect in 2D aerial photographs [8]. This also made it possible to calculate volumetric and not just planimetric changes in beaches and dunes. In addition, with LiDAR technology and photogrammetry, there has been a progress toward higher density and accuracy of measurement and results.

The first part of this chapter is devoted to a technical and conceptual synthesis. A bibliometric analysis shows the recent, rapid, and phased success of the use of GNSS, LiDAR, and then airborne photogrammetry in the field of coastal geomorphology. We will briefly describe the techniques, emphasizing their complementarities and their spatial and temporal scales of application. The second part of this chapter is an illustration of the first by selected examples of results obtained on the coast of northern France. The conclusion proposes a synthesis of the advantages and disadvantages of these techniques and discusses some future prospects.

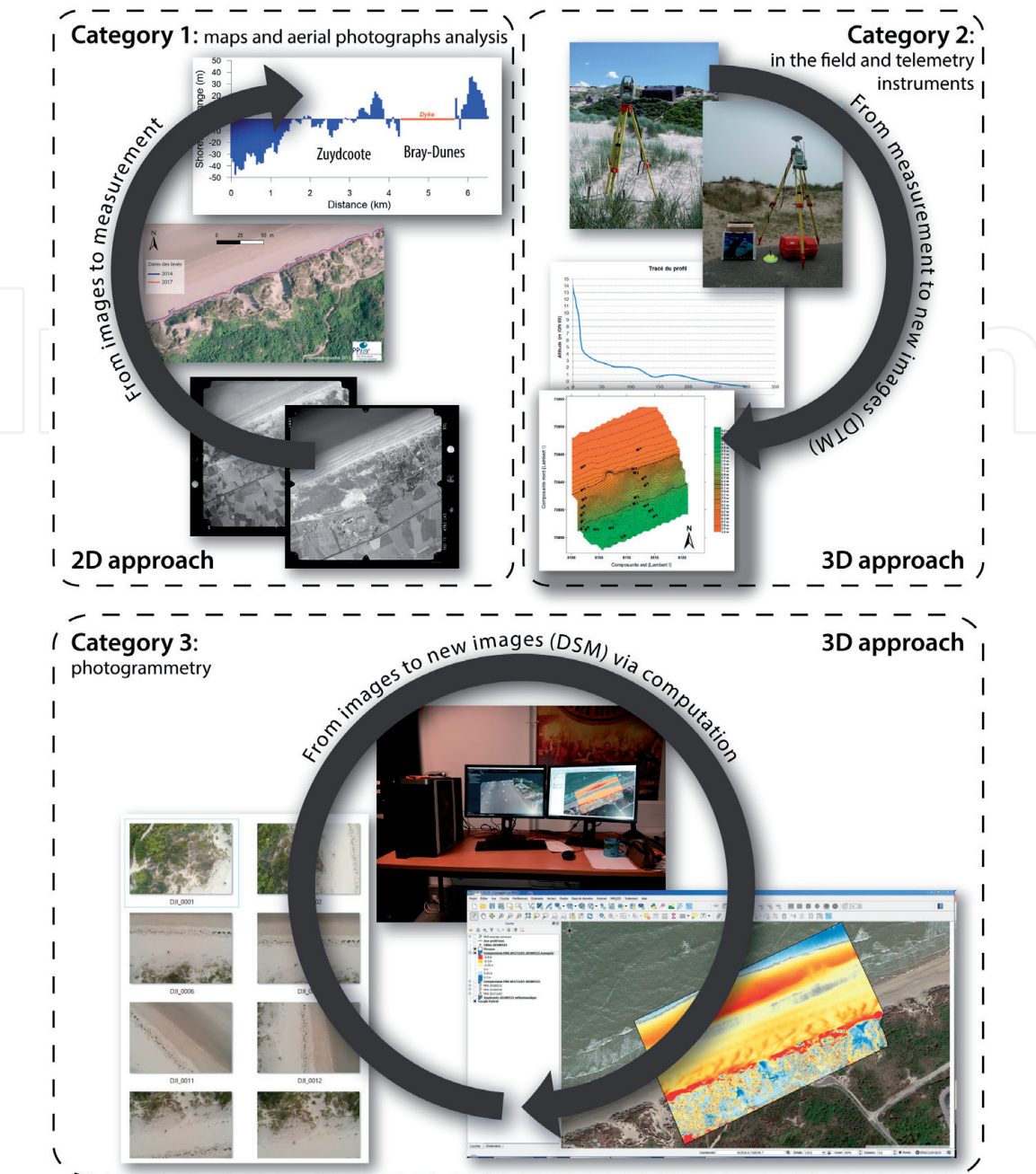


Figure 1.
The measurement method paradigm.

2. From GNSS to LiDAR and photogrammetry: three successful technologies aiming to a higher density of measurements

The use of these three techniques in Earth and environmental sciences began about 30 years ago. They have achieved rapid and phased success as they have been further developed and progressively introduced.

2.1 A rapid growth in the use of these techniques

2.1.1 In environmental sciences

In environmental sciences, the applications of these three techniques are very diverse and operate at different spatial scales.

Differential GNSS is an in-situ measurement system that is used in all areas where an accurate position on the planet's surface is required [9]. With GNSS, for example, time series of measurements can be made at fixed locations, for example, to identify the role of vertical movements of the continent in changes in relative sea level [10] or to map the plate boundary faults [11]. Multiple point measurements are also frequently taken at different locations and interpolated to produce elevation maps, for example, for glacial geomorphological mapping [12].

Light Detection and Ranging (LiDAR) is a telemetry system (remote measurement) that can be used in two main configurations: on the ground with TLS systems and in airborne configuration. As shown in a bibliometric study in the field of earth sciences in Ref. [13], the Terrestrial Laser Scanning (TLS) technique is used to make precise topographic surveys at distance without having to come into contact with the ground, which is very convenient in hard-to-reach terrain such as steep cliffs. Very large numbers of measurements can be made with these instruments, which allow to model the investigated object. Fields of investigation using the techniques are, for example, at fine-scale mineralogy and petrology and at a larger scale structural geology, seismology, volcanology, tsunami hazards, geomorphology, and cryosphere studies [13]. Airborne LiDAR is used to produce accurate elevation maps at a larger scale, usually over large areas. The spectrum of applications in the Earth and ecological sciences is wide [14], for example, for lava flow survey [15] and forestry [16, 17].

Photogrammetry can also be implemented at different scales, from very fine scale, over a few millimeters, for example, to monitor the rock surface weathering [18], to medium scale, over areas ranging from a few thousand square meters to a few hectares, for example, to monitor the evolution of slopes [19, 20] or coastal habitats [21–23]. Finally, it can be deployed on a large scale, over areas of several square kilometers (e.g., geomorphological mapping in high mountain environment) [24].

2.1.2 In coastal geomorphology over the past 25 years

In order to estimate the development of these three techniques in coastal geomorphology in particular, a bibliometric analysis was conducted following a method similar to that of [13] for the use of TLS in Earth sciences and [25] for UAVs in agriculture and forestry.

The Scopus database was used for finding publications (articles and book chapters) in the field of Earth and planetary sciences, from 1995 to 2019, searching for the following keywords: the kind of instrument (gps or dgps or gnss or dgnss/ LiDAR/uav or uas or drone), coast or beach or dune or shoreline. Early results often contained intruders (e.g., in the military, maritime navigation, biology, mathematics, or electronic fields). It was therefore necessary to reduce the research panel by excluding keywords and certain journals outside the field of coastal geomorphology.

Figure 2 shows the results of this analysis for the three types of techniques. It can be seen that GNSS was used earlier than the other two techniques. This is logical since it is the first of the three technologies that have been developed. However, during the last years, the number of mentions of satellite positioning systems decreases. This is probably not because they are less used, rather because they have become commonly used and authors probably no longer feel the need to describe or even mention the technique in the publication. However, these GNSSs are still needed for complementing LiDARs and UAVs.

The LiDAR citation curve reflects the development of this technology during the last decades. In the second half of the 1990s, there are a limited number of publications in which the tool is experimental or is used by only a few organizations that

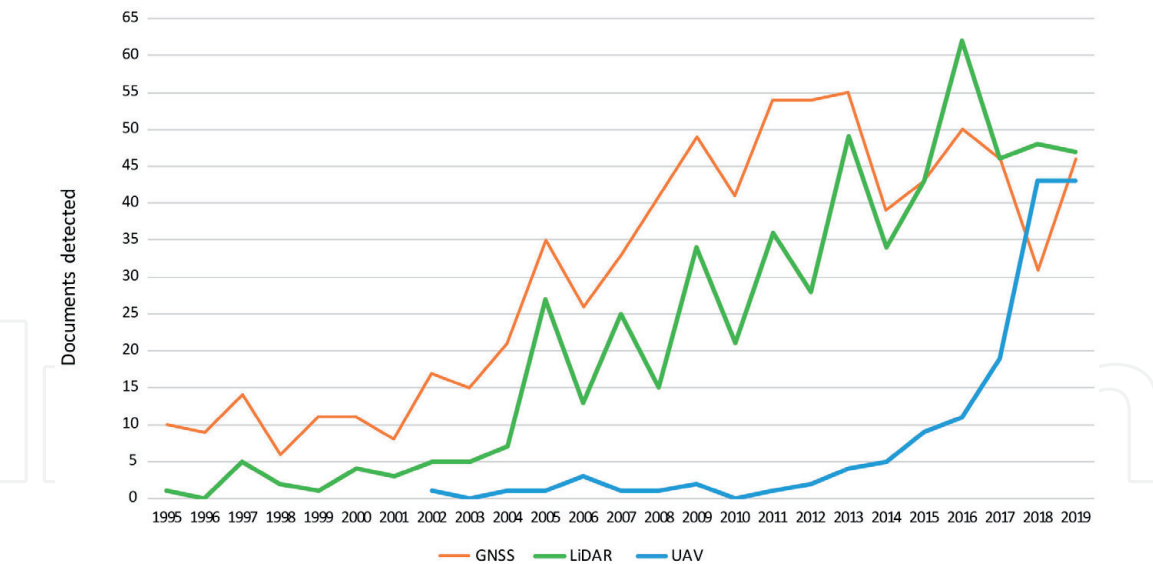


Figure 2.
Results of the bibliometric analysis on GNSS, LiDAR, and UAV mentions from 1995 to 2019.

have the technical and financial means to use it (e.g., US Army Corps of Engineers USACE) [26]. This technique significantly increased at the beginning of the 2000s whether airborne or TLS (e.g., for monitoring the evolution of cliffs) [27–29]. The use of UAVs did not begin until the early 2000s. This technique took off during the second decade of the twenty-first century with the availability of light aircraft (<2 kg), ready to fly, simple to program and pilot, and financially affordable [22]. UAVs are most often used for photogrammetry (see below) and more rarely to carry small LiDAR systems [30] or multispectral sensors [31]. It is interesting to note that, at the end of the study period, the three techniques are almost equal in terms of citations in the literature: although the use of UAVs started late, it is now as common as that of GNSS and LiDAR.

2.2 The use of these techniques in coastal geomorphology

2.2.1 Differential GNSS

Global Navigation Satellite Systems (GNSSs), more commonly known by the acronym GPS, make it possible to measure a position in three dimensions, anywhere on the Earth's surface, using the trilateration principle (with three satellites) [32], that is, by referring to the very precisely known positions of the satellites in their orbits. The use of a radio beacon precisely geo-referenced on land, installed near the study site and communicating with the GNSS receiver via UHF waves, makes it possible to reduce the error margin of measurement, which ranges from several millimeters to centimeters, or even millimeters both horizontally and vertically.

During fieldwork campaigns, when numerous measurements for generating accurate Digital Terrain Model are required, the RTK (Real Time Kinematic) mode is generally used: the GNSS automatically records elevation data points during the operator's movements following a previously defined time step or distance.

Elevation point measurements can be acquired on foot when the areas to be covered are fairly small (a few thousand square meters or even a few hectares) or with an all-terrain vehicle (e.g., a quad where the GNSS is mounted coupled to an inertial station to compensate for the vehicle's movements) driving slowly (between 10 and 20 km/h) for larger and fairly flat areas. Although larger areas can be covered with a vehicle, the density of points collected is rather low. In the example shown in **Figure 3**, the elevation data points were collected using a Leica 1200 GNSS, which

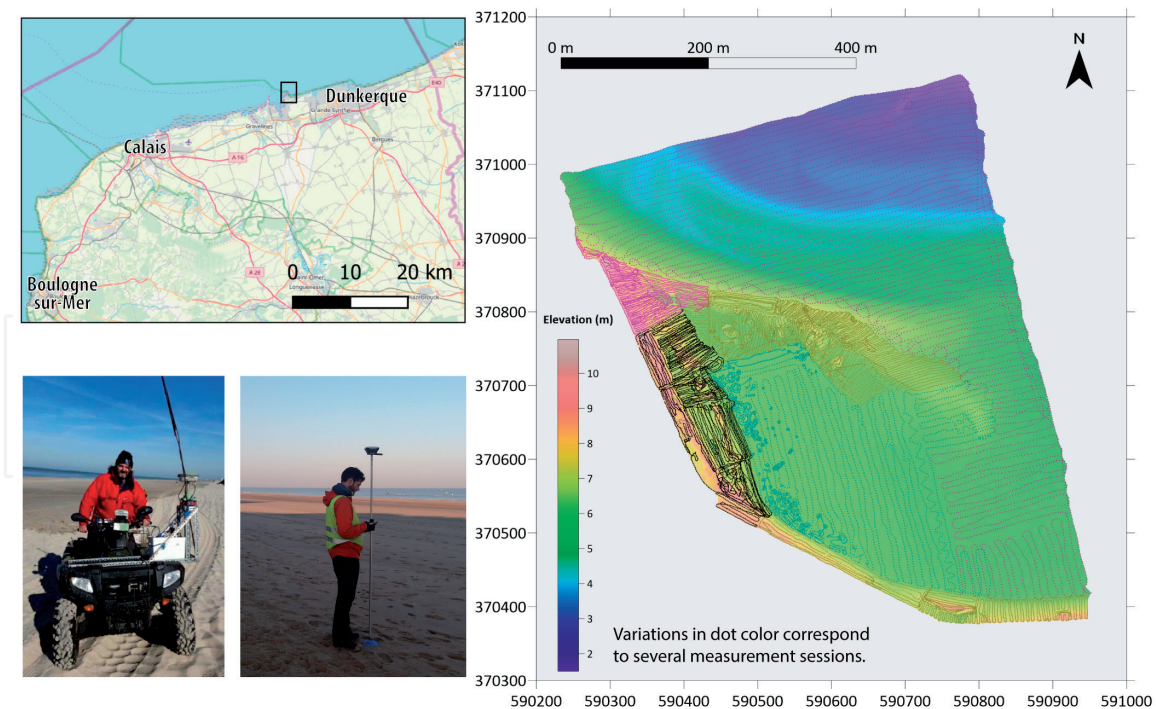


Figure 3.

In the field topographic survey using a GNSS; example of a DTM (the measurement points are overlapped on the DTM).

accuracy is ± 1.5 cm horizontally and ± 3 cm vertically, coupled to an inertial station SBG 500-E on a quad. The DTM was calculated by triangulation of Delaunay along the coastline of the port of Dunkirk. The measured points were superimposed on it. The intertidal zone was measured with a GNSS receiver of an all-terrain vehicle; the alignments of the points along the vehicle's trajectory are clearly visible. The upper beach, the foredune, the muddy areas, and the sand and pebble spit were measured on foot because the relief is too constraining for the vehicle; foot surveys enable higher measurement densities. This type of topographic survey is time-consuming: for a survey of 36,360 points, over a surface area of 33.5 ha, resulting in a measurement density of 0.1 point per m^2 , it took 5 days of work during daytime and low tide periods.

2.2.2 Airborne LiDAR

Airborne LiDAR is an active telemetry instrument. A vector, aircraft [33–35], helicopter, or UAV [30, 36] whose position and altitude are precisely determined using a differential GNNS, carries a side-scanning laser that emits pulses under the vector. The laser beam is emitted toward the ground; the round-trip time of this beam and its “echo” is measured. The speed of propagation of the beam is perfectly known according to the atmospheric conditions (temperature and humidity). For each point aimed at on the ground, several signals are recorded and averaged: this is the distance between the device and the ground surface. Ground control points are checked with GNSS to calibrate the data as accurately as possible.

Airborne LiDAR surveys can provide a large number of measurements over large areas of several square kilometers. The measurement density is higher than that obtained with in situ GNNS. It can typically range from 1 to 2 points/ m^2 , for example, from 1.2 to 1.4 points/ m^2 after data filtering [37, 38]. In the example shown in **Figure 4**, a Leica HawkEye III topo-bathymetric LiDAR sensor was used with a 500 KHz frequency in infrared spectrum for topographical surveying and a 35 KHz frequency in the green spectrum for bathymetric monitoring in shallow

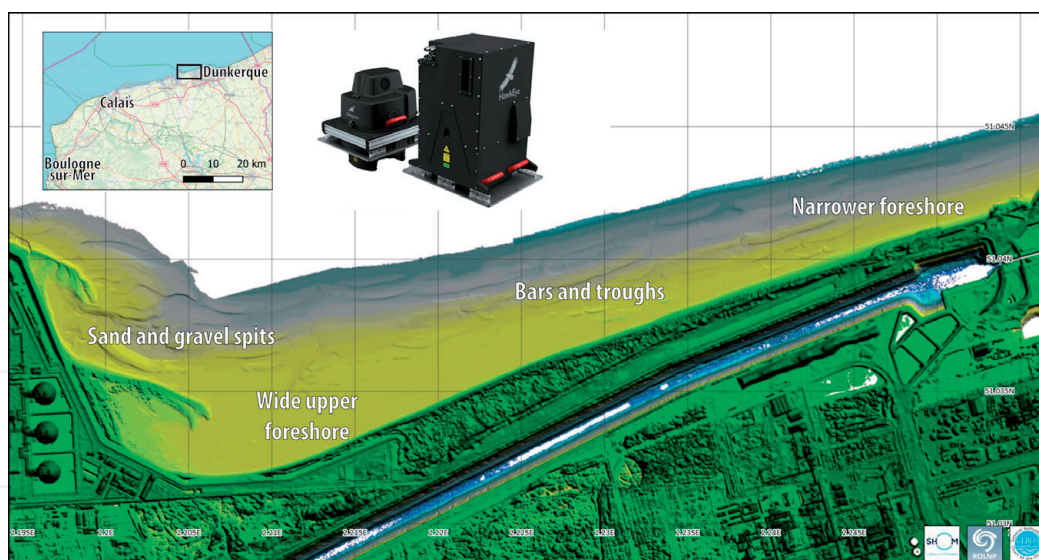


Figure 4.
 Extract of an extensive 1 m spatial resolution DTM on the harbor of Dunkirk coast, northern France carried out with a Leica HawkEye III LiDAR (sources: map SHOM, ROLNP on data.shom.fr; picture, Leica Geosystems).

water. The density of topographical measurements is 12 points/m² before data filtering. According to the manufacturer, the measurement accuracy is ± 20 cm horizontally and ± 2 cm vertically. This vertical margin of error is generally noted on bare surfaces (sand and rock) but increases significantly in vegetated areas (25 cm).

Maps produced from LiDAR data are Digital Surface Models (DSM) that show the top of all objects. These DSMs represent the ground relief in bare areas (beach and rocky plains) but may show the tops of vegetation or buildings elsewhere. In geomorphology, however, the object of the study is the relief on the ground and not that on the surface of the vegetation or other objects. To obtain a Digital Terrain Model (DTM), buildings can be removed by using a vector map of the building to delineate the areas of the points to be deleted. At the location of each building, an interpolation is then made with the ground elevations around the perimeter of the building. For vegetated areas, the data are filtered: the first echo of the signal is considered as the one corresponding to the surface of the objects, and the last echo (the furthest from the vector) is assimilated to the ground. DTMs are therefore calculated using the last echoes resulting in lower measurement densities. However, the vegetation is sometimes too dense for the LiDAR signal to reach the ground and for a DTM to be extracted from the DSM; this is notably the case in coastal dunes covered by sea buckthorn (**Figure 4**). DSMs or DTMs are calculated by interpolation from points; they can be represented in vector mode as contour maps or in raster mode where each pixel contains elevation information. With a data point density of 1–2 points/m², there is no need to aim for a spatial resolution of DSM or DTM finer than 1 m/pixel. **Figure 4** shows the very wide foreshore along the port of Dunkirk, which gradually narrows toward the east. It also shows a morphology of bars and troughs on the foreshore. The sand and gravel spits are clearly visible.

2.2.3 Airborne photogrammetry

Photogrammetry is a nonactive telemetry process because no signal is emitted. It can be defined simply as the “science of making reliable measurements from photographs” [39]. It is most frequently applied to aerial photographs. It allows distance and surface measurements to be made in plan. It is also possible to extract altitude information from two vertical aerial photographs of the same area taken from different angles using the principle of stereoscopy.

Photogrammetry therefore requires a camera: formerly, a silver camera, and nowadays, a high-resolution digital sensor. These cameras are embarked on different types of carriers: airplanes [40], ultralight aircraft [41], or UAV [42–46]. The cameras are installed on stabilized gimbals that compensate for the vector's pitch and roll movements in order to minimize the blurring effects on the photographs.

“Conventional” airborne photogrammetry, using carriers flying at altitudes of 500–5000 m above the ground, provides results with highly variable vertical error margins that largely depend on the spatial resolution of the acquired images and therefore on the flying height. The margin of error can be metric (1.5 m in mountainous areas) [24] or decimetric (30 cm in coastal areas) [39], which is not accurate enough to detect fine detail and small amplitude changes on beaches.

In recent years, airborne photogrammetry by UAV at low altitude (below 150 m) and very high spatial resolution has rapidly gained popularity in coastal geomorphology. As mentioned above, this success has been made possible by the development of digital photogrammetry and the introduction of small, easy-to-use, and affordable civilian UAVs. This success is also due to a technical change in photogrammetry, which was originally only an optical technique, requiring the use of bulky equipment and the permanent intervention of a technician, whereas it is now completely digital and can be automated almost all along the image processing workflow. Specialized software, but relatively easy to use for those who are familiar with geomatics, is available. These programs perform a correspondence analysis of the pixels of the images to “stitch” them together like a panorama; they calculate angles between the shooting points and these pixels in order to calculate depths of field or differences in altitude to represent the relief.

The protocol for organizing a UAV photogrammetry mission is simple. A flight plan is programmed, which forecasts the UAV's trajectory in the form of flight path parallel to each other in the area to be studied. The flight altitude of the aircraft is parameterized, which, depending on the sensor's fineness, determines the spatial resolution of the vertical images: the greater the height, the lower the resolution. For example, with a 20 MPixel sensor, a pixel of 2.41 μm , a focal length of 8.8 mm (DJI Phantom IV Pro or Mavic 2 Pro UAV), a flight height of 50 m, the spatial resolution of an image will be 1.4 cm/pixel.

$$R = H \times 100 \times \left[\frac{P \times 10^{-4}}{F \times 10^{-1}} \right] \quad (1)$$

where R is the spatial resolution of the image in cm/pixel, H is the flying height in meters, P is the sensor pixel size in microns, and F is the sensor focal length in millimeters.

Overlap between two successive photographs and lateral overlap between two parallel strips of photographs are programmed (80 and 60% are recommended, respectively). On the UAV's speed depends on these parameters. The speed must be slow enough to avoid blurring on the photographs. In the example shown in **Figure 5**, the flight height of the DJI Mavic 2 Pro was 65 m, and the speed was 5 m/s. Oblique aerial photographs can also be integrated into the data to be processed: they help to better model steep slope reliefs such as cliffs or foredune fronts. The flight plan is recorded and used for repeated overflights at different dates. During each campaign, ground control points, evenly distributed over the study area, are measured using GNSS. The coordinates of these control points allow the DSM to be set very precisely in plan and in altitude.

Digital photogrammetric processing with very high spatial resolution allows to generate a very high density of measurement points and to calculate very fine DSMs. The DTM, as shown in **Figure 5**, was calculated with an average density of 269 points/ m^2 . The average error margin of the measurements is 3.2 cm in the plane and

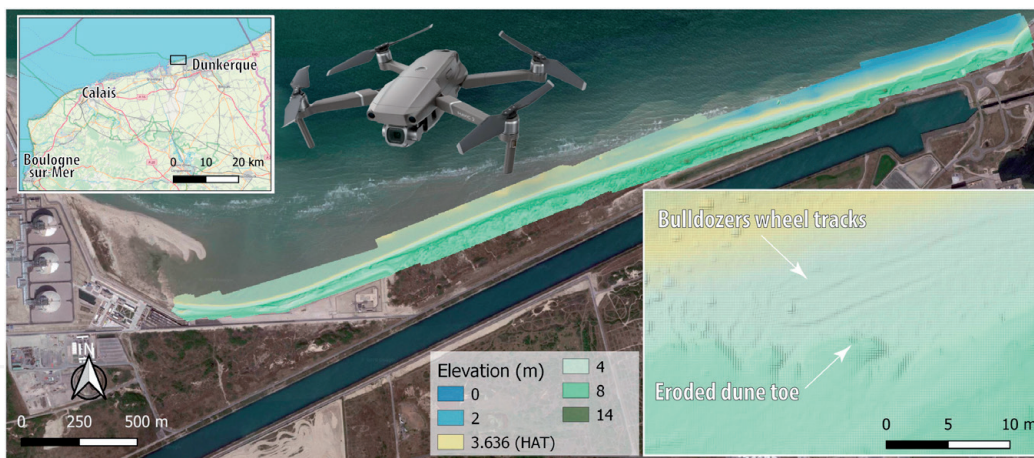


Figure 5.
 Example of a very high resolution DSM computed from photogrammetric survey carried out with a DJI Mavic 2 Pro UAV on the harbor of Dunkirk coast, northern France.

2.5 cm at altitude with a spatial resolution of 6 cm/pixel. The sharpness is such that when zooming in, wheel tracks of bulldozers replenishing the beach a little further east can be seen. Such spatial resolution of the DSM can be achieved, thanks to the very high density of the points. As with LiDAR data, photogrammetric measurements concern the surface of objects: the transformation of DSMs into DTMs is sometimes possible for spatially well-defined objects (buildings and small groves of vegetation) using the same methods. However, such high accuracy DTMs can hardly be obtained in densely vegetated areas. Interpretations of elevation changes must then be very cautious. An apparent increase in altitude may be the consequence of vegetation growth and not of sand accretion (see Section 3 of this chapter).

A major interest of photogrammetry compared to LiDAR is that it allows the acquisition of aerial photographs on which many detailed observations can be distinguished (e.g., sand/vegetation limit on the upper beach and type of vegetation). These photographs, each covering a small area, can be assembled to form a full orthophotograph [39]. They are corrected for optical distortions using precisely known shooting parameters and recorded in the exif metadata of the files; distortions due to relief are corrected using DSM.

2.3 Synthesis

GNSS, LiDAR, and photogrammetry can be classified in several ways. A distinction can be made between ground (GNSS and TLS) and airborne (LiDAR and photogrammetry) measurement methods, active (sending/receiving a signal; GNSS, TLS, and LiDAR) and nonactive (photogrammetry) measurement methods, in situ (GNSS) and telemetry (remote measurement, TLS, LiDAR, and photogrammetry) measurement methods.

The quality of the results is closely linked to the positioning accuracy at the different stages of the technical protocols (e.g., TLS, vector, and ground control points) and therefore to GNSS, which remains an essential instrument for the calibration of the elevation data.

The graph in **Figure 6** aims at showing the complementarity of these techniques. Two parameters are taken into account: on the abscissa, the time scale/frequency of acquisition, and on the ordinate, the spatial density of the measurements, which is a key factor for the accuracy of DTMs or DSMs [47]. As the frequency of data acquisition increases and the degree of accuracy becomes more refined, finer analyses become possible. With regularly repeated high spatial resolution DSMs, it is thus

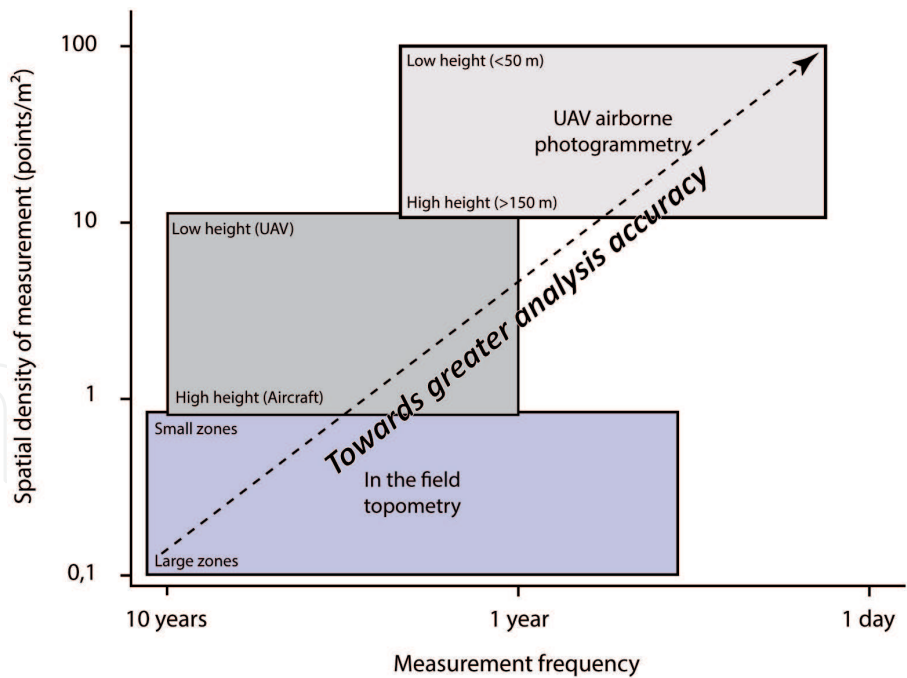


Figure 6.
Spatial and temporal scales of application of the three techniques.

possible to highlight otherwise undetectable detail changes at lower acquisition frequency and/or with coarser spatial resolution surveys (e.g., aeolian sand accumulations, see Section 2 of this chapter).

3. Case studies: shoreline changes on the coasts of northern France

The second part of the chapter presents examples of studies carried out on the northern coast of France in the surrounding of Dunkirk. Topographic surveys were carried out using differential GNSS, LiDAR, and airborne photogrammetry. These examples illustrate the benefits of changing from two- to three-dimensional analysis and improving spatial resolution.

3.1 Toward a more accurate coastline detection

The shoreline is the indicator most often used to define, map the position of the shore, and study its evolution [48]. There are several definitions of shoreline [8]. The definition may vary according to the coastal environments studied, for example, the boundary between water and sand in a microtidal environment, the base of the top of a cliff, the berm of a pebble barrier, the toe of coastal dunes, and the boundary between sand and beach top vegetation. Along the same coast, the position of these different shoreline indicators does not always coincide: for example, the limit between sand and vegetation may be located several meters away landward of the dune toe (**Figure 7**). The definition of the coastline is therefore an essential prerequisite in diachronic analyses of the shoreline.

Identifying the shoreline in two dimensions on aerial photographs is sometimes difficult. On aerial photographs, whether historical or recent, the coastline is not always clearly distinguishable. **Figure 7** shows two aerial photographs shot at two different dates (1957 and 2015), at the same scale. On the 1957 photo of poor quality, the break in slope is hardly detectable where the foredune slope is gentle. In GIS analyses, an error margin in detection must be taken into account ($\pm x$ pixels,

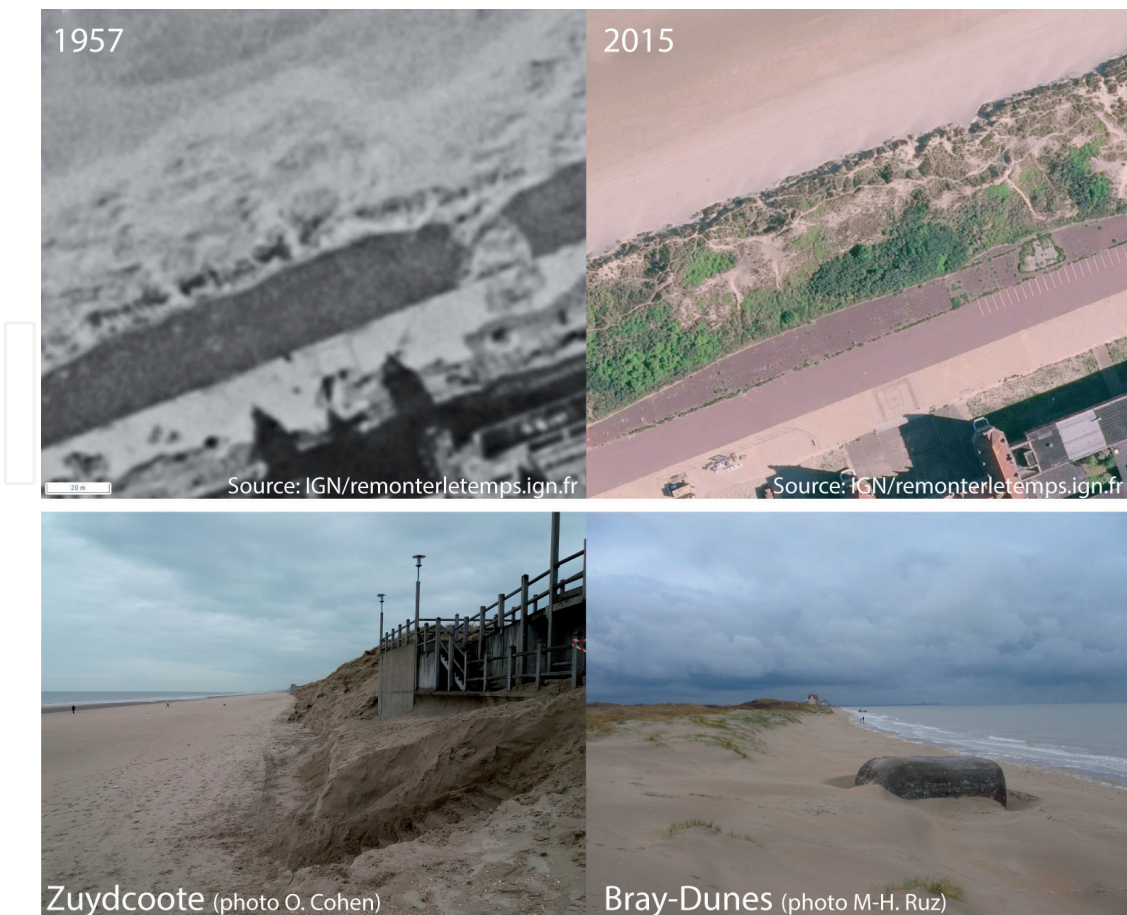


Figure 7.
 The complex detection of the shoreline on aerial photographs and in the field.

thus $\pm y$ m, depending on the spatial resolution of the digitized photos) [49]. Stereoscopic observation of paper photos helps to identify the shoreline position, but the transfer of these observations to a computer is not convenient. Computer and photogrammetric processing of the images improves analysis (see below).

The shoreline can be measured in the field by GNSS. This requires a clear definition of what is considered as a shoreline and a good experience in field investigation. In the following examples along the coasts of northern France, the dune toe was selected. The shoreline is easily detected when the dune toe is marked by a sharp change in slope gradient (e.g., in Zuydcoote in **Figure 7**), but not when the slope between the upper beach and the dune is mild and regular (e.g., in Bray-Dunes). The measurement accuracy of GNSS is high, but in these cases, an error margin has to be attributed to the operator's interpretation of the terrain.

The shoreline can be defined by an altitude level, for example, the one reached by a distinct tide level such as the mean high spring tide. This approach is used by the French National Hydrographic and Oceanographic Service (SHOM) to define the official coastline in France, called “Histolitt,” which corresponds to the highest astronomical tide (HAT). Along the coastline east of Dunkirk, for example, the HAT corresponds to an altitude of 3.787 m (French elevation datum), which has been mapped on a recent DSM obtained from an aerial photogrammetric survey with a high spatial resolution (5 cm/pixel) carried out in September 2019. The “Histolitt” shoreline has also been superimposed on the 2019 DSM showing an offset of about 11 m between the two shorelines (**Figure 8**) even if the shoreline position was defined by the same altitudinal level (3.787 m) in both cases. This difference in position between the two shorelines can be explained by the fact that the “Histolitt” shoreline was determined from a DTM with a vertical accuracy of

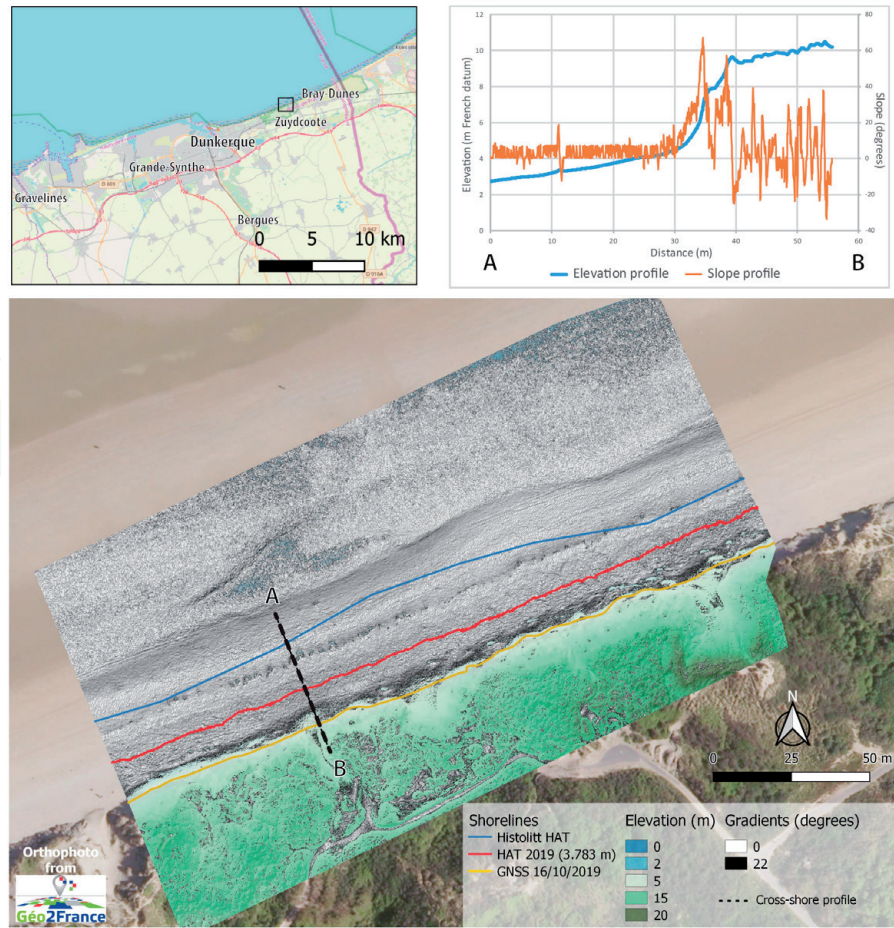


Figure 8.

Example of shoreline detection on a DTM/DSM and comparison with the shoreline measured by GNSS in the field.

50 cm calculated by photogrammetry with aerial photographs of 2004. The recent fine-scale mapping of the upper beach and coastal dunes shows that the “Histolitt” shoreline is now outdated since its position does not correspond to the present day morphology anymore. Nevertheless, even if the updated shoreline position using the location of the HAT level on the recent DSM is more consistent with the actual present day shoreline, its position still lays several meters seaward of the dune toe (**Figure 8**) that is the geomorphological expression of the upper limit of action of the highest water levels, including tides and meteorological surges related to wind and changes in atmospheric pressure [38].

The shoreline may also be mapped in a semi-automatic way by identifying in a DTM for a neat variation of the slope gradient at the dune toe [38] using the following approach:

$$\left\| \vec{g} \right\| = \sqrt{\left(\frac{\partial z}{\partial x} \right)^2 + \left(\frac{\partial z}{\partial y} \right)^2} \quad (2)$$

where g is the slope gradient, z is the altitude, and x and y are the planar coordinates of each pixel in the DTM. **Figure 8** shows a slope gradient map calculated from a DSM computed by photogrammetry in September 2019 in Zuydcoote. The figure also exhibits two cross-sectional profiles: one is a topographic profile, and the other is a slope gradient profile in degrees. In this example, a slope gradient of 22° corresponding to the dune toe has been selected. On the map, areas with slopes between 0 and 22° range from light to dark grey. They are mainly located on the beach; there are, however, some areas with low gradients in the coastal dunes

(e.g., paths). Zones with steeper slopes are not displayed on the map; therefore, the actual topography remains visible. The detection of this boundary is validated by comparison with the coastline surveyed in October 2019 with a GNSS: the differences range from 0 to 2.5 m landward, which are due to beach and dune toe erosion between September and October 2019, as a result of high water levels that had eroded the beach and the foot of the dune.

Figure 9 illustrates a diachronic study using shorelines extracted from DTMs at different dates (2008, 2011, 2012, and 2014) on an 8 km long stretch of coast between Dunkirk and the Belgian border. The analysis of the shoreline evolution from 2008 to 2014 indicates a clear contrast between the sectors west and east of Bray-Dunes. However, the meteorological and marine conditions (winds and water levels) were the same throughout the study area [50]. The first sector is characterized by a general but moderate progradation (a few meters) from 2008 to 2011 and 2012 and from 2012 to 2014 by a mean erosion of 6 m, up to 10 m in some sectors. The second sector east of Bray-Dunes underwent accretion over all the study period with a mean seaward migration of the shoreline of 10 m: it is especially noticeable from 2008 to 2011 and 2012 and is more moderate for the last period from 2012 to 2014 where some sectors even experienced mild erosion.

3.2 Calculation of altimetric and volumetric changes

Switching from 2D to 3D analysis enables to detect the shoreline position more accurately. 3D analysis using DTMs or DSMs also allows volume calculation and mapping of topographic changes. On sandy coasts, this approach can be used for calculating sediment volume changes and sediment budgets and for mapping accretionary and eroding sectors that are potentially at risk [51]. Below are two examples at two different scales on the coast east of Dunkirk.

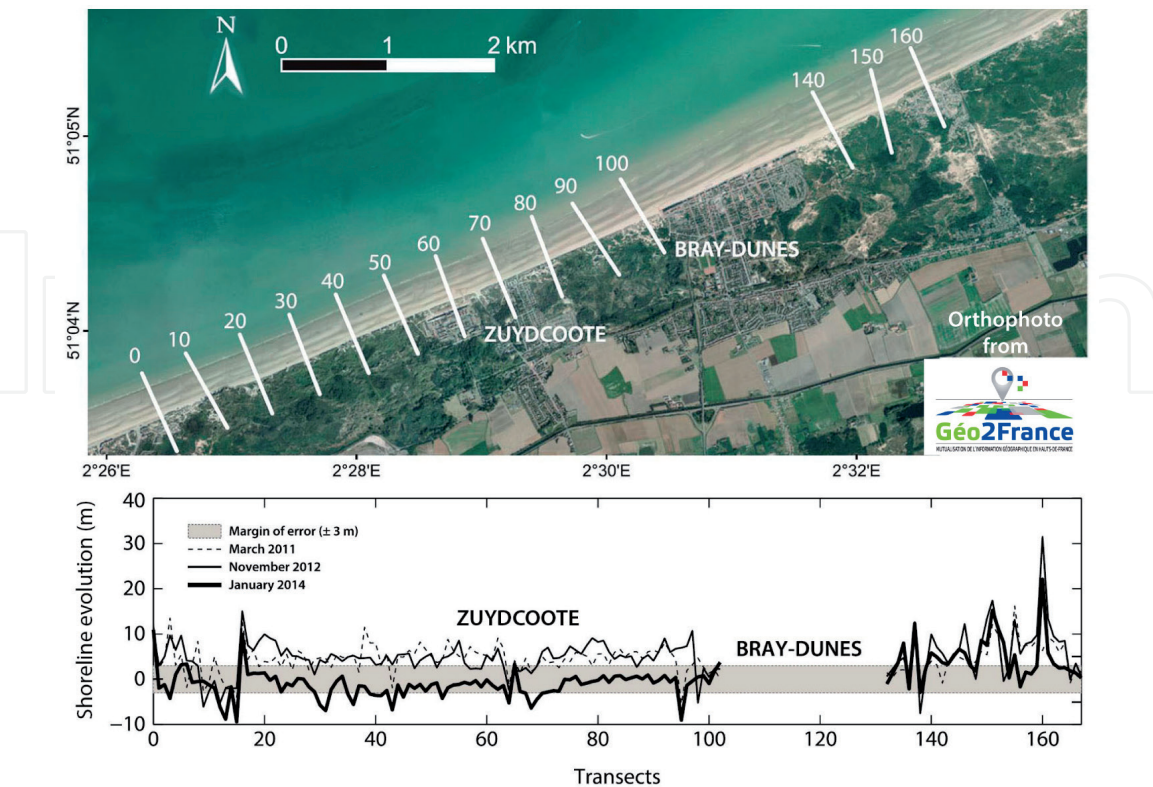


Figure 9.
Evolution of the shoreline in Dunkirk and the Belgian border from 2008 to 2014 with transect location map (adapted from Ref. [38]).

3.2.1 Very high spatial resolution and short-term shoreline analysis at Zuydcoote

Four photogrammetric survey campaigns were carried out in November 2017, May 2018, September 2018, and February 2019. Very high spatial resolution DSMs were then calculated (5 cm/pixel; **Figure 10a**). The DSMs were compared in pairs (e.g., **Figure 10b**). In order to synthesize the four DSMs, a statistical analysis was also conducted. For example, a map of the annual rate of change was produced by calculating a linear regression with the pixel heights at each date.

For example, between November 2017 and May 2018, the sediment budget was negative (-5041 m^3 , i.e., $-0.15\text{ m}^3/\text{m}^2$), 1368 m^3 ($0.22\text{ m}^3/\text{m}^2$) of sediment accumulated, and 6410 m^3 was eroded ($-0.25\text{ m}^3/\text{m}^2$). Erosion was very mainly detected on the beach and dune front. The comparison map of the DSMs (**Figure 10b**) shows a flattening of the upper intertidal bar and the upper foreshore, and the disappearance of the aeolian sand accumulation features identified on the DSM of November 2017 (**Figure 10a**). The DSM comparison also shows that the dune front has been eroding, although blowouts were filling up.

The map of the annual rate of change calculated with the four DSMs (**Figure 10c**) confirms the previous observations: erosion of the sand bar, upper beach and dune front, and accumulation in the trough landward of the upper intertidal bar and in the blowouts. The topographic and statistical cross-shore profiles (**Figure 10d**) show that the highest negative evolution rates are corresponding to the foredune front. As indicated in Section 2.2.3 of this chapter, such map must be interpreted with caution. In bare areas, the geomorphological analysis can be validated, but in the vegetated zones, the changes detected may be due to vegetation growth and not to geomorphological changes. The interpretation of these DSMs must therefore always be combined with observation of aerial photographs.

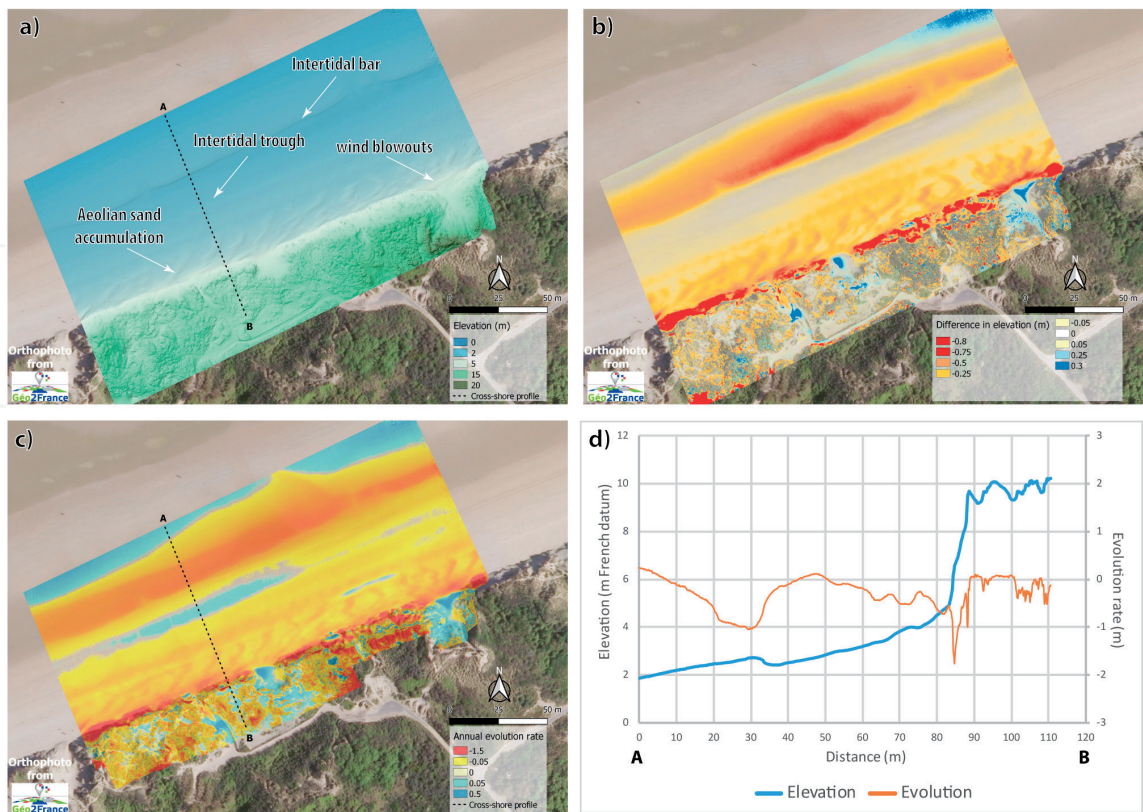


Figure 10. Examples of (a) DSM computed from photogrammetry data (November 2017), (b) evolution map (November 2017 to May 2018), (c) map of annual rate of evolution, and (d) cross-shore topographical and evolution rate profiles.

3.2.2 Large-scale calculation of the sediment budget east of Dunkirk

Four topographic survey campaigns were carried out with an airborne topographic LiDAR in May 2008, March 2011, November 2012, and January 2014 on a 8 km long coastal stretch east of Dunkirk. For each measurement campaign, a DTM with a spatial resolution of 1 m was calculated. In order to understand sediment transfer between beach and dunes, these DTMs were used to calculate sediment volume variations in the mid foreshore, upper beach, and dune (**Figure 11**). The lower foreshore limit corresponds to the minimum elevation at the time of LiDAR measurements and therefore depends on the tidal level. The upper limit of the mid foreshore is the Mean High Water level (MHW, 2.83 m French elevation datum at Dunkirk). The upper beach is the area between the MHW level and the shoreline determined using the gradient method (see Section 3.1). The seaward limit of the dunes is the shoreline, whereas the inner limit is determined by photo-interpretation according to the type of dune vegetation identified in order to exclude areas with high vegetation (e.g., sea buckthorn) where the differences between the DTM and the actual ground topography may exceed 50 cm.

Figure 11 shows that the shoreline east of Dunkirk experienced a sediment accumulation of approximately $326 \times 10^3 \text{ m}^3$ from 2008 to 2014. Almost half of this accumulation is observed in the coastal dunes ($154 \times 10^3 \text{ m}^3$), mainly in the eastern part, next to the Belgian border. The average vertical accretion is 1 m. In the whole study zone where the shoreline has been stable from 2008 to 2014, the sediment budget of the dunes is positive even if dune front erosion occurred in places. Estimates of changes in sediment volume indicate that accumulation in coastal dunes occurred primarily prior to erosive events in the fall and winter of 2013, particularly between 2008 and 2011 when a gain of more than $122 \times 10^3 \text{ m}^3$

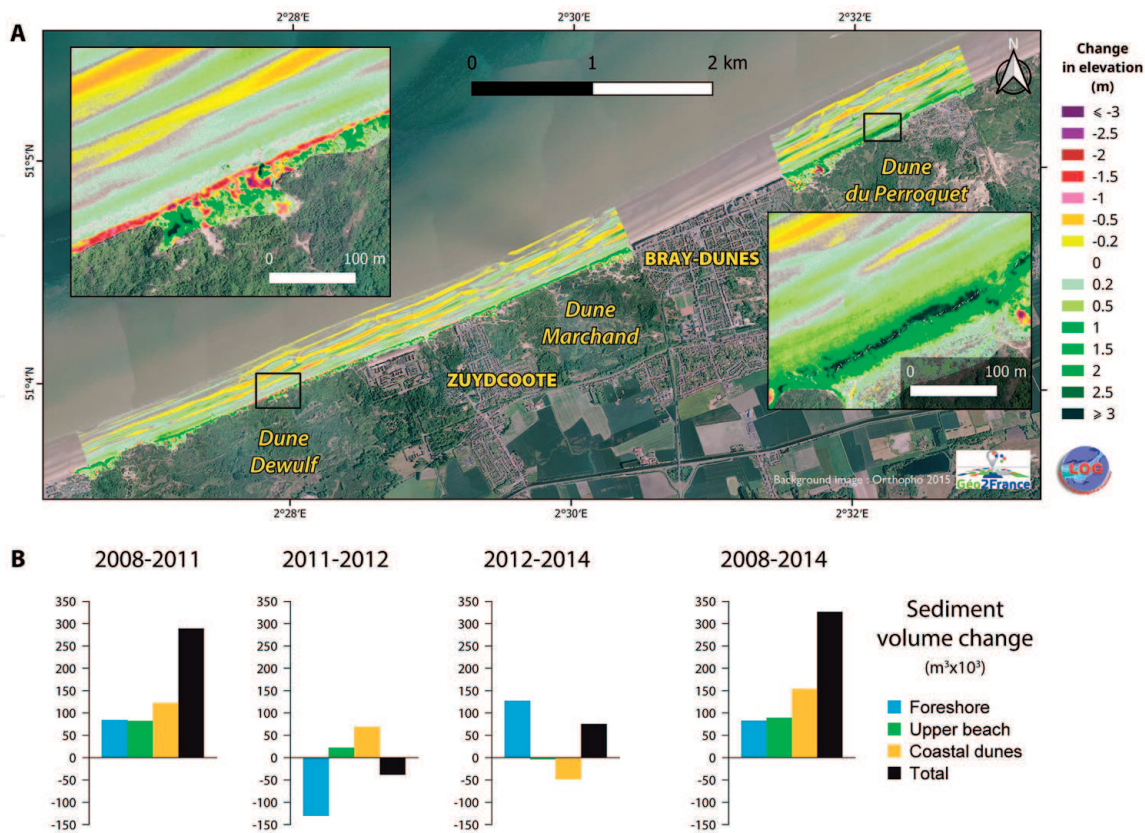


Figure 11.
(A) Map of shore evolution between Dunkirk and the Belgian border from 2008 to 2014 and (B) volumetric evolution of the foreshore, upper beach, and dunes (adapted from Ref. [38]).

of sand was observed. Sediment accumulation was about $69 \times 10^3 \text{ m}^3$ in the coastal dunes during the following period (2011–2012), which corresponds to a constant average accumulation rate of about $0.13 \text{ m}^3/\text{m}^2/\text{year}$ in the dunes during both periods. Subsequently, storms in late 2013 [50] resulted in widespread coastal retreat associated with the erosion of coastal dunes west of Bray-Dunes (**Figure 11**). About $36.5 \times 10^3 \text{ m}^3$ and $15.7 \times 10^3 \text{ m}^3$ were eroded from the Dune Dewulf and the Dune Marchand, respectively, between 2012 and 2014. However, the Perroquet Dune, east of Bray-Dunes, remained fairly stable or even accumulated slightly during this storm period. Although coastal dune erosion was significant during the 2012–2014 period, a comparison of the 2008 and 2014 DTMs shows an accumulation in the dunes almost everywhere along the coast (**Figure 11A**) due to the supply of aeolian sand from the beach. Such vertical accretion is visible even where coastal dune erosion has occurred (e.g., Dune Dewulf), suggesting that wind-blown sand may also have been transported landward as the dune front eroded and retreated.

The upper part of the beach was also characterized by accretion along most of the study site, with a total gain of nearly $90 \times 10^3 \text{ m}^3$ between 2008 and 2014, with maximum accumulation ($>0.5 \text{ m}$) measured in the eastern part of the study site (**Figure 11B**). As for the dunes, sand accumulation on the upper beach occurred mainly between 2008 and 2012, while slight erosion occurred locally between 2012 and 2014. Comparison of the 2008 and 2014 DTMs shows characteristic patterns of topographic change of intertidal bars and troughs on the foreshore. The corresponding volume changes are very limited: about $+83 \times 10^3 \text{ m}^3$ over the whole foreshore, corresponding to only $0.04 \text{ m}^3/\text{m}^2$.

4. Conclusions

This synthesis showed that the new topographic measurement techniques implemented in coastal geomorphology over the last 25 years had enabled a clear gain in productivity in topographic measurements. The density of measurements has considerably increased, for example, for areas of several hectares, from $0.1 \text{ points}/\text{m}^2$ to $1\text{--}2 \text{ points}/\text{m}^2$ with LiDAR and several hundred points/ m^2 with photogrammetry. This greater density of points resulted in the calculation of DTMs or DSMs with a higher spatial resolution ($1 \text{ m}/\text{pixel}$ with LiDAR measurements, $5 \text{ cm}/\text{pixel}$ for photogrammetric measurements) on which small-scale landforms and topographic changes that could not be distinguished at a coarser resolution can be detected. With the development of these new techniques, it is therefore nowadays possible to work on shoreline morphodynamics at a very fine scale. For example, aeolian sand accumulation landforms on the upper beach and dune blowouts associated with pedestrian trampling are visible on a photogrammetric DSM but not on a LiDAR DTM (**Figure 12**: on the left, extract of the LiDAR DTM, and on the right, the photogrammetry DSM).

This improvement in spatial resolution is also associated with a decrease in measurement error margins ($\pm 20 \text{ cm}$ horizontally and 2 cm vertically for aircraft LiDAR measurements, $\pm 3 \text{ cm}$ in both dimensions for low-height photogrammetric UAV surveys), which results in a higher accuracy of the DTMs produced.

Table 1 compares the advantages and disadvantages of the three techniques. The financial costs are not discussed here.

In the coming years, coastal geomorphologists are waiting for a technique that will automatically distinguish bare areas from vegetated areas, so that DTMs can be easily calculated. The simultaneous use of LiDAR and multi- and hyperspectral sensors on board aircraft [52] or UAVs [31] is an interesting prospect. These multi- and hyperspectral images, processed with remote sensing methods, allow to

map vegetation and soil moisture. This is particularly interesting for analyzing the dynamics of embryo dunes, which is closely linked to the development of pioneer vegetation [53] or monitoring the stabilization or restoration of established coastal dunes [54].

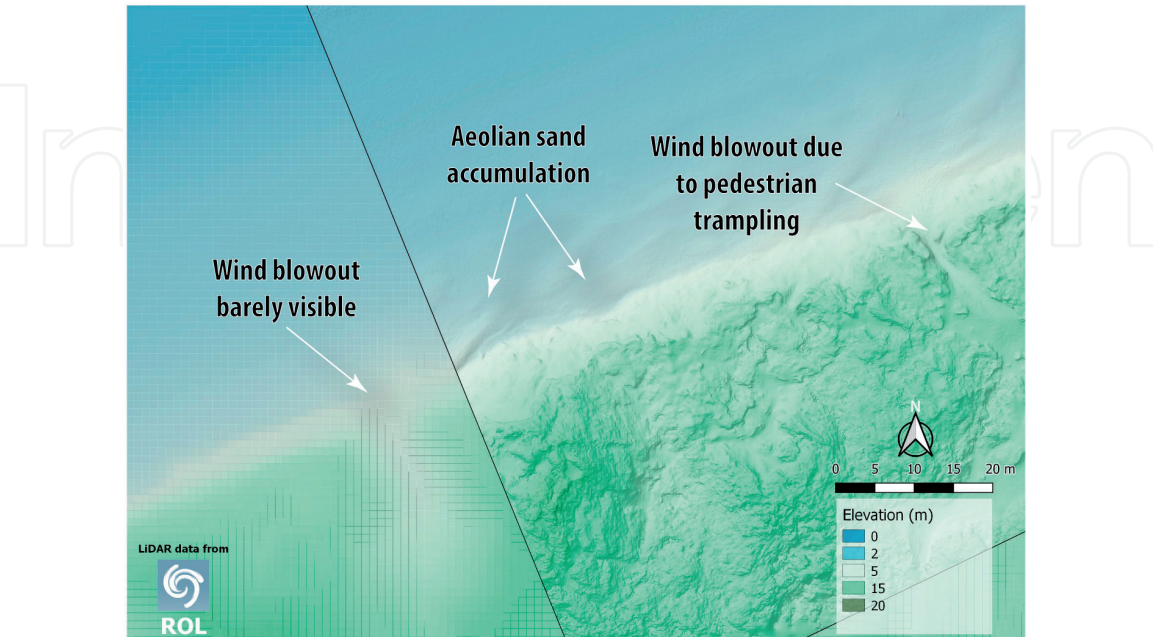


Figure 12.
Comparison of DSM calculated from LiDAR data (on the left) and low-height photogrammetry (on the right).

Technique	Advantages	Disadvantages
GNSS	Measurement campaign very easy to organize High repeatability Not really sensitive to weather conditions High accuracy measurements Short processing time of the data Small to medium amount of data to be stored Provide DTM	Fit for small to medium study zones Only provide topographical measurement Low measurement density Time consuming measurements
UAV photogrammetry	Fit for small to medium study zones (short flight time and limited range) Measurement campaign easy to organize (depending on local regulations) High repeatability High measurement density High accuracy measurement Provide full orthophotographs for photointerpretation	Sensitive to weather conditions Long processing time of the data and high computing power required Huge amount of data to be stored Provide DSM, difficult to compute DTM
Airborne LiDAR	Fit for large study zones (extensive flight range) Medium measurement density Can provide DTM	Measurement campaign difficult to organize Low repeatability Medium accuracy measurement Sensitive to weather conditions Long processing time of the data and high computing power required Huge amount of data to be stored

Table 1.
Advantages and disadvantages of the three techniques.

Acknowledgements


The LiDAR surveys mentioned in this chapter were carried out within the framework of the interregional project CLAREC (2008–2013) coordinated by the University of Caen (France). The 2017 LiDAR data were provided by the Interregional Coastal Monitoring Network (Réseau d’Observation du Littoral Normandie Hauts-de-France ROL). The photogrammetric survey instruments were acquired, thanks to an equipment grant (BQR) from Université du Littoral Côte d’Opale. Shoreline monitoring and photogrammetric surveys on the coastline east of Dunkirk are carried out within the framework of National Observation Service DYNALIT (www.dynalit.fr). The authors would like to thank Denis Marin for his help in the realization of several figures.

Author details

Olivier Cohen* and Arnaud Héquette
Oceanology and Geosciences Laboratory, Université du Littoral Côte d’Opale,
Université de Lille, CNRS, UMR 8187, Wimereux, France

*Address all correspondence to: olivier.cohen@univ-littoral.fr

IntechOpen

© 2020 The Author(s). Licensee IntechOpen. This chapter is distributed under the terms of the Creative Commons Attribution License (<http://creativecommons.org/licenses/by/3.0>), which permits unrestricted use, distribution, and reproduction in any medium, provided the original work is properly cited. 

References

- [1] Masselink G, Hughes MG. An Introduction to Coastal Processes and Geomorphology. 2nd ed. London: Routledge; 2014. p. 432
- [2] Davidson-Arnott R, Bauer B, Houser C. Introduction to Coastal Processes and Geomorphology. Cambridge: Cambridge University Press; 2019. p. 541
- [3] Cohen O, Gardel A. De l'analyse des cartes anciennes à l'altimétrie laser aéroportée: L'évolution des techniques de suivi du trait de côte. Exemples sur la Côte d'Opale. In: Schmitt F, editor. Observation des écosystèmes marin et terrestre de la Côte d'Opale: Du naturalisme à l'écologie. Paris: Union des Océanographes Français; 2011. pp. 153-169
- [4] Cohen O. La baie de Fréjus: 2000 ans d'évolution du rivage. Mappemonde. 1997;1(1):6-12
- [5] Fenster MS, Dolan R, Elder JF. A new method for predicting shoreline positions from historical data. Journal of Coastal Research. 1993;9(1):147-171
- [6] Hesp PA, Ruz M-H, Hequette A, Marin D, Miot da Silva G. Geomorphology and dynamics of a traveling cusped foreland, Authie estuary, France. Geomorphology. 2016;254:104-120
- [7] Zemmour A. Étude de l'évolution des littoraux dunaires de la Côte d'Opale à différentes échelles de temps: Analyse de leur capacité de régénération post-tempête [PhD thesis]. Université du Littoral Côte d'Opale; 2019. Available from: <https://tel.archives-ouvertes.fr/tel-02270709>
- [8] Boak EH, Turner IL. Shoreline definition and detection: A review. Journal of Coastal Research. 2005;214:688-703
- [9] Perosanz F. GNSS: A revolution for precise geopositioning. Comptes Rendus Physique. 2019;20(3):171-175
- [10] Cheng H-Q, Chen J-Y. Adapting cities to sea level rise: A perspective from Chinese deltas. Advances in Climate Change Research. 2017;8(2):130-136
- [11] Donnellan A, Arrowsmith R, DeLong S. Spatio-temporal mapping of plate boundary faults in California using geodetic imaging. Geosciences (Switzerland). 2017;7(1):26
- [12] Chandler BMP, Lovell H, Boston CM, Lukas S, Barr ID, Benediktsson ÍÖ, et al. Glacial geomorphological mapping: A review of approaches and frameworks for best practice. Earth-Science Reviews. 2018;185:806-846
- [13] Telling J, Lyda A, Hartzell P, Glennie C. Review of Earth science research using terrestrial laser scanning. Earth-Science Reviews. 2017;169:35-68
- [14] Eitel JUH, Höfle B, Vierling LA, Abellán A, Asner GP, Deems JS, et al. Beyond 3-D: The new spectrum of lidar applications for earth and ecological sciences. Remote Sensing of Environment. 2016;186:372-392
- [15] Crown DA, Anderson SW, Finnegan DC, LeWinter AL, Ramsey MS. Topographic and thermal investigations of active pahoehoe lava flows: Implications for planetary volcanic processes from terrestrial analogue studies. In: 44th Lunar and Planetary Science Conference. Vol. 44. 2013. p. 2184
- [16] Wulder MA, White JC, Nelson RF, Næsset E, Ørka HO, Coops NC, et al. Lidar sampling for large-area forest characterization: A review. Remote Sensing of Environment. 2012;121:196-209

- [17] Beland M, Parker G, Sparrow B, Harding D, Chasmer L, Phinn S, et al. On promoting the use of lidar systems in forest ecosystem research. *Forest Ecology and Management*. 2019;**450**:117484
- [18] Verma AK, Bourke MC. A method based on structure-from-motion photogrammetry to generate sub-millimetre-resolution digital elevation models for investigating rock breakdown features. *Earth Surf Dynamics*. 2019;**7**(1):45-66
- [19] Westoby MJ, Brasington J, Glasser NF, Hambrey MJ, Reynolds JM. 'Structure-from-Motion' photogrammetry: A low-cost, effective tool for geoscience applications. *Geomorphology*. 2012;**179**: 300-314
- [20] Stöcker C, Eltner A, Karrasch P. Measuring gullies by synergetic application of UAV and close range photogrammetry—A case study from Andalusia, Spain. *CATENA*. 2015;**132**:1-11
- [21] Leon JX, Roelfsema CM, Saunders MI, Phinn SR. Measuring coral reef terrain roughness using 'Structure-from-Motion' close-range photogrammetry. *Geomorphology*. 2015;**242**:21-28
- [22] Ventura D, Bonifazi A, Gravina MF, Ardizzone GD. Unmanned aerial systems (UASs) for environmental monitoring: A review with applications in coastal habitats. In: Mejia ODL, Gomez JAE, editors. *Aerial Robots—Aerodynamics, Control and Applications*. Rijeka: IntechOpen; 2017. Available from: <http://www.intechopen.com/books/aerial-robots-aerodynamics-control-and-applications/unmanned-aerial-systems-uass-for-environmental-monitoring-a-review-with-applications-in-coastal-habi>
- [23] Ventura D, Bruno M, Jona Lasinio G, Belluscio A, Ardizzone G. A low-cost drone based application for identifying and mapping of coastal fish nursery grounds. *Estuarine, Coastal and Shelf Science*. 2016;**171**:85-98
- [24] Müller J, Gärtner-Roer I, Thee P, Ginzler C. Accuracy assessment of airborne photogrammetrically derived high-resolution digital elevation models in a high mountain environment. *ISPRS Journal of Photogrammetry and Remote Sensing*. 2014;**98**:58-69
- [25] Raparelli E, Bajocco S. A bibliometric analysis on the use of unmanned aerial vehicles in agricultural and forestry studies. *International Journal of Remote Sensing*. 2019;**40**(24):9070-9083
- [26] Lillycrop WJ, Estep LL. Generational advancements in coastal surveying, mapping. *Sea Technology*. 1995;**36**(6):10-15
- [27] O'Neal MA. Terrestrial laser scanner surveying in coastal settings. *Coastal Research Library*. 2014;**9**:65-76
- [28] Mazzanti P, Schilirò L, Martino S, Antonielli B, Brizi E, Brunetti A, et al. The contribution of terrestrial laser scanning to the analysis of cliff slope stability in Sugano (Central Italy). *Remote Sensing*. 2018;**10**(9):3
- [29] Letortu P, Costa S, Maquaire O, Davidson R. Marine and subaerial controls of coastal chalk cliff erosion in Normandy (France) based on a 7-year laser scanner monitoring. *Geomorphology*. 2019;**335**:76-91
- [30] Lin Y-C, Cheng Y-T, Zhou T, Ravi R, Hasheminasab SM, Flatt JE, et al. Evaluation of UAV LiDAR for mapping coastal environments. *Remote Sensing*. 2019;**11**(24):32
- [31] Suo C, McGovern E, Gilmer A. Coastal dune vegetation mapping using a multispectral sensor mounted on an UAS. *Remote Sensing*. 2019;**11**(15)

- [32] Boeser SM. Global positioning systems (GPS). In: Finkl CW, Makowski C, editors. *Encyclopedia of Coastal Science* [Internet]. Cham: Springer International Publishing; 2019. pp. 905-907
- [33] Brock JC, Purkis SJ. The emerging role of lidar remote sensing in coastal research and resource management. *Journal of Coastal Research*. 2009;**10053**:1-5
- [34] Debaine F, Robin M. A new GIS modelling of coastal dune protection services against physical coastal hazards. *Ocean & Coastal Management*. 2012;**63**:43-54
- [35] Le Mauff B, Juigner M, Ba A, Robin M, Launeau P, Fattal P. Coastal monitoring solutions of the geomorphological response of beach-dune systems using multi-temporal LiDAR datasets (Vendée coast, France). *Geomorphology*. 2018;**304**:121-140
- [36] Shaw L, Helmholz P, Belton D, Addy N. Comparison of UAV LiDAR and imagery for beach monitoring. *International Archives of the Photogrammetry, Remote Sensing and Spatial Information Sciences*. 2019;**XLII-2/W13**:589-596
- [37] Levoy F, Anthony EJ, Monfort O, Robin N, Bretel P. Formation and migration of transverse bars along a tidal sandy coast deduced from multi-temporal Lidar datasets. *Marine Geology*. 2013;**342**:39-52
- [38] Crapoulet A, Héquette A, Marin D, Levoy F, Bretel P. Variations in the response of the dune coast of northern France to major storms as a function of available beach sediment volume: Response of Dune Coast to Storm as a Function of Beach Sediment Volume. *Earth Surface Processes and Landforms*. 2017;**42**(11):1603-1622
- [39] Thieler ER, Hapke CJ. Photogrammetry. In: Finkl CW, Makowski C, editors. *Encyclopedia of Coastal Science* [Internet]. Cham: Springer International Publishing; 2019. pp. 1367-1374
- [40] Hapke C, Richmond B. Monitoring beach morphology changes using small-format aerial photography and digital softcopy photogrammetry. *Environmental Geosciences*. 2000;**7**(1):32-37
- [41] Brunier G, Fleury J, Anthony EJ, Gardel A, Dussouillez P. Close-range airborne structure-from-motion photogrammetry for high-resolution beach morphometric surveys: Examples from an embayed rotating beach. *Geomorphology*. 2016;**261**:76-88
- [42] Casella E, Rovere A, Pedroncini A, Mucerino L, Casella M, Cusati LA, et al. Study of wave runup using numerical models and low-altitude aerial photogrammetry: A tool for coastal management. *Estuarine, Coastal and Shelf Science*. 2014;**149**:160-167
- [43] Gonçalves JA, Henriques R. UAV photogrammetry for topographic monitoring of coastal areas. *ISPRS Journal of Photogrammetry and Remote Sensing*. 2015;**104**:101-111
- [44] Turner IL, Harley MD, Drummond CD. UAVs for coastal surveying. *Coastal Engineering*. 2016;**114**:19-24
- [45] Pikelj K, Ružić I, Ilić S, James MR, Kordić B. Implementing an efficient beach erosion monitoring system for coastal management in Croatia. *Ocean & Coastal Management*. 2018;**156**:223-238
- [46] Laporte-Fauret Q, Marieu V, Castelle B, Michalet R, Bujan S, Rosebery D. Low-cost UAV for high-resolution and large-scale coastal dune change monitoring using photogrammetry. *Journal of Marine Science and Engineering*. 2019;**7**(3):63

[47] Grohmann CH, Sawakuchi AO. Influence of cell size on volume calculation using digital terrain models: A case of coastal dune fields. *Geomorphology*. 2013;**180-181**:130-136

[48] Pérez-Alberti A, Pires A, Chaminé HI. Shoreline and coastal terrain mapping. In: Finkl CW, Makowski C, editors. *Encyclopedia of Coastal Science*. Cham: Springer International Publishing; 2019. pp. 1558-1571

[49] Thieler ER, Danforth WW. Historical shoreline mapping (I): Improving techniques and reducing positioning errors. *Journal of Coastal Research*. 1994;**10**(3):549-563

[50] Héquette A, Ruz M-H, Zemmour A, Marin D, Cartier A, Sipka V. Alongshore variability in coastal dune erosion and post-storm recovery, Northern Coast of France. *Journal of Coastal Research*. 2019;**SI88**:25-45

[51] List J. Sediment budget. In: Finkl CW, Makowski C, editors. *Encyclopedia of Coastal Science*. Cham: Springer International Publishing; 2019. pp. 1505-1512

[52] Deronde B, Houthuys R, Debruyn W, Fransaer D, Lancker VV, Henriët J-P. Use of airborne hyperspectral data and laserscan data to study beach morphodynamics along the Belgian Coast. *Journal of Coastal Research*. 2006;**225**:1108-1117

[53] Ruz M-H, Héquette A, Marin D, Sipka V, Crapoulet A, Cartier A. Development of an incipient foredune field along a prograding macrotidal shoreline, northern France. *Géomorphologie: Relief, Processus, Environnement*. 2017;**23**(1):37-50

[54] Martinez LM, Gallego-Fernández JB, Hesp PA, editors. *Restoration of Coastal Dunes*. Berlin Heidelberg: Springer-Verlag; 2013. p. 347